ACS APPLIED MATERIALS & INTERFACES

www.acsami.org

Research Article

Tunable Thermoelectric Performance of the Nanocomposites Formed by Diketopyrrolopyrrole/Isoindigo-Based Donor−Acceptor Random Conjugated Copolymers and Carbon Nanotubes

Kuan-Chieh Wang,[#] Po-Shen Lin,[#] Yan-Cheng Lin,[*,#] Shih-Huang Tung, Wen-Chang Chen, and Cheng-Liang Liu[*]

Cite This: *ACS Appl. Mater. Interfaces* 2023, 15, 56116−56126

Read Online

ACCESS | Metrics & More | Article Recommendations | Supporting Information

ABSTRACT: This paper presents the development of thermoelectric properties in nanocomposites comprising donor−acceptor random conjugated copolymers and single-walled carbon nanotubes (SWCNTs). The composition of the conjugated polymers, specifically the ratio of diketopyrrolopyrrole (DPP) to isoindigo (IID), is manipulated to design a series of random conjugated copolymers (DPP0, DPP5, DPP10, DPP30, DPP50, DPP90, DPP95, and DPP100). The objective is to improve the dispersion of SWCNTs into smaller bundles, leading to enhanced thermoelectric properties of the polymer/SWCNT nanocomposite. This dispersion strategy promotes an interconnected conducting network, which plays a critical role in optimizing the thermoelectric performance. Accordingly, the effects of morphologies on the thermoelectric properties of the nanocomposites are systematically investigated. The DPP95/SWCNT nanocomposite exhibits the strongest interaction, resulting in the highest power factor (PF) of 711.1 μW m^{-1} K^{-2}, derived from the high electrical conductivity of 1690 S cm^{-1} and Seebeck coefficient of 64.8 μV K^{-1}. The prototype flexible thermoelectric generators assembled with a DPP95/SWCNT film achieve a maximum power output of 20.4 μW m^{-2} at a temperature difference of 29.3 K. These findings highlight the potential of manipulating the composition of random conjugated copolymers and incorporating SWCNTs to efficiently harvest low-grade waste heat in wearable thermoelectric devices.

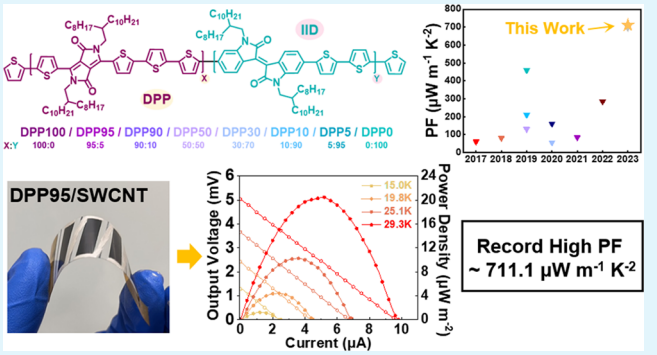

KEYWORDS: *thermoelectrics, conjugated polymers, carbon nanotubes, nanocomposite, donor−acceptor*

INTRODUCTION

Thermoelectric materials have garnered significant attention in recent years due to their potential for use in power generation and refrigeration applications.[1−7] However, traditional inorganic thermoelectric materials have limitations such as high cost, brittleness, toxicity, and complexity in processing, despite their excellent thermoelectric properties.[8−10] To address these challenges, organic thermoelectric materials have emerged as a promising alternative, thanks to their cost-effectiveness, low thermal conductivity (κ), and mechanical flexibility, which make them suitable for use in wearable thermoelectric generators (TEGs).[11−16] The thermoelectric figure of merit ($ZT = \sigma S^2 T/\kappa$) is a crucial metric for evaluating thermoelectric performance, taking into account electrical conductivity (σ), Seebeck coefficient (S), κ, and absolute temperature (T). Organic-based materials are known for their low κ, and as such, enhancing the thermoelectric power factor ($PF = \sigma S^2$) has been a primary focus of research on organic thermoelectric materials.[17−20]

However, most existing organic thermoelectric materials suffer from a trade-off between σ and κ, which limits their overall efficiency. To address this limitation, conjugated polymers and carbon nanotubes (CNTs) have been developed as thermoelectric nanocomposites, creating specific charge carrier pathways that enhance S without compromising σ.[21−30] While various conjugated polymers such as poly(3,4-ethylenedioxythiophene) (PEDOT),[31−33] polyaniline (PANI),[34,35] polypyrrole (PPy),[36] and poly(3-hexylthiophene) (P3HT)[37,38] have been investigated for their thermoelectric properties in composites with CNTs, donor−acceptor (D−A) conjugated polymers are considered particularly promising due to their stronger intermolecular interaction and higher electron affinity.

Received: August 11, 2023
Revised: November 8, 2023
Accepted: November 10, 2023
Published: November 27, 2023

https://doi.org/10.1021/acsami.3c11792
ACS Appl. Mater. Interfaces 2023, 15, 56116−56126

Table 1. Summary of Thermoelectric Parameters of the D−A Conjugated Polymer/SWCNT Nanocomposites Investigated in This Work and Those Reported in Recent Literature[39−48]

nanocomposite	casting method	σ [S cm^{-1}]	S [μV K^{-1}]	PF [μW m^{-1} K^{-2}]	ref
PDPPSe/SWCNT	mold	538	62.5	210	43
PBDTDTffBT/SWCNT	drop-casting	529	68.1	80.9	44
PCDTPT/FWCNT	drop-casting	760	76.0	459.1	45
PCDTFBT/FWCNT	drop-casting	798	69.9	397.5	45
CDTBTZ/FWCNT	drop-casting	782	71.7	409	45
IDTBT/CNT	spin-coating	854	90.9	697	46
CF_3−SAM/SWCNT	drop-casting	825	58.8	285	47
P(DTCBT)/SWCNT	drop-casting	187	50	44	48
P(DTSiBT)/SWCNT	drop-casting	294	54	77	48
P(DTOBT)/SWCNT	drop-casting	245	58.9	85	48
PBDT-EDOT/SWCNT	drop-casting	360	40	60.8	49
PBDT-C-BT/SWCNT	drop-casting	110	68	56	50
P(IDTBT-EG)/SWCNT	drop-casting	3393	23	161.3	51
P(IDTBT)/SWCNT	drop-casting	3283	20	139	51
P(TBT-Pt)/SWCNT	drop-casting	666	44.3	130.7	52
P(TBT)/SWCNT	drop-casting	864.4	26.2	59.5	52
DPP100/SWCNT	spin-coating	397.7	60.7	147.5	this work
DPP95/SWCNT	spin-coating	1689.7	64.8	711.1	this work
DPP90/SWCNT	spin-coating	1135.8	63.5	459.2	this work
DPP50/SWCNT	spin-coating	811.4	61.2	305.0	this work
DPP30/SWCNT	spin-coating	712.2	61.1	266.7	this work
DPP10/SWCNT	spin-coating	278.7	66.3	170.7	this work
DPP5/SWCNT	spin-coating	212.2	68.3	111.4	this work
DPP0/SWCNT	spin-coating	470.9	59.9	173.8	this work

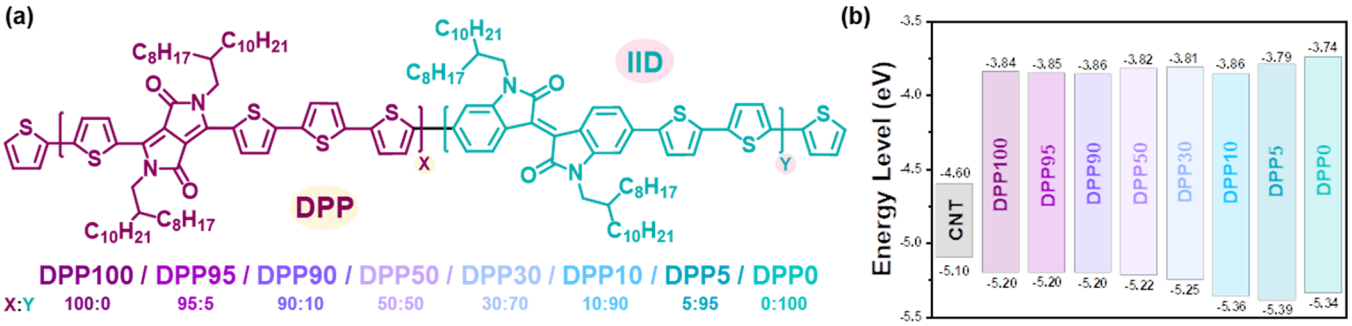

Figure 1. (a) Molecular structures of the random conjugated copolymers containing DPP and IID moieties with different X:Y compositions. (b) Energy level diagrams comparing the investigated random conjugated copolymers and SWCNTs.

Wang et al. conducted a study in which they designed a novel donor−acceptor conjugated polymer, based on benzo-[1,2-b:4,5-b′]-dithiophene (BDP), named PBDTDTffBT, and investigated its effect on thermoelectric properties by varying the mass ratios of PBDTDTffBT to SWCNTs. The nanocomposite films obtained at a mass ratio of 1:10 between PBDTDTffBT and SWCNTs demonstrated a maximum PF of 80.9 μW m^{-1} K^{-2}.[39] Wan et al. proposed that the insertion of platinum acetylides into π-conjugated polymers can effectively enhance the S and lead to a PF of 130.7 μW m^{-1} K^{-2} for polymer/SWCNT hybrid thermoelectric systems.[40] Kang et al. discovered that planar-shaped poly(diketopyrrolopyrrole-selenophene) (PDPPSe), which exhibits strong π−π interaction, can align with CNTs in an in-plane direction, leading to a dense surface microstructure that enhances σ and yields higher PF values of 210 μW m^{-1} K^{-2}.[41] Chen et al. conducted a study where they incorporated polar ethylene glycol ether side chains into the backbone of an indacenodithiophene-benzothiodazole conjugated polymer to construct thermoelectric polymer/SWCNT nanocomposites, exhibiting a high PF value of 161.3 μW m^{-1} K^{-2}. The inclusion of polar side chains is attributed to the stronger bond energy and formation of enhanced van der Waals forces, contributing to the improved performance of the nanocomposites.[42] Jung et al. discovered that the strong intermolecular interaction forces and high backbone planarity of the cyclopentadithiophene (CDT) donor, in conjugation with the acceptor units of pyridyl-thiadiazole, known as PCDTPT, facilitated an efficient debundling of few-walled carbon nanotubes (FWCNTs) by wrapping around their surface. This interaction resulted in significantly reduced bundle sizes of the FWCNTs. Consequently, the PCDTPT/FWCNT composite films showed superior thermoelectric performances with an improved PF of up to 459 μW m^{-1} K^{-2}.[43] Figure S1 illustrates the progress made in enhancing PF values for donor−acceptor conjugated polymer/SWCNT nanocomposites, and Table 1 summarizes the various processing methods used to prepare nanocomposite films and their thermoelectric performance.[39−48] However, few studies have investigated the carrier-filtering effect in nanocomposites consisting of low bandgap polymers.[49−58] There-

https://doi.org/10.1021/acsami.3c11792
ACS Appl. Mater. Interfaces 2023, 15, 56116−56126

fore, it is essential to develop D−A conjugated polymers with appropriate energy levels for use in thermoelectric nanocomposite systems in order to investigate the impact of efficient carrier filtering on thermoelectric properties.

In this study, a series of D−A random conjugated copolymers consisting of diketopyrrolopyrrole (DPP) and isoindigo (IID) conjugated moieties were designed, and eight different polymers were prepared by varying the IID contents from 0 to 100%. The polymers were named DPP100 to DPP95, DPP90, DPP50, DPP30, DPP10, DPP5, and DPP0, with IID contents of 0 to 5, 10, 30, 50, 90, 95, and 100%, respectively.[59] The chemical structures of the random conjugated copolymers used for their thermoelectric nanocomposite with SWCNTs are shown in Figure 1a. DPP and IID are similar in the dimensions of chemical structures, thereby providing decent compatibility with each other during random copolymerization and solid-state stacking. Previous reports have shown that random conjugated copolymers with low IID content, such as DPP95 and DPP90, exhibit superior electrical properties due to the improved interchain packing and solid-state aggregation compared to DPP100,[59] making them highly desirable for thermoelectric applications. The energy level of the DPP/IID-based random conjugated copolymers can be tailored by varying the IID content. Furthermore, the introduction of a low IID content increases the $\pi-\pi$ interaction between copolymers (DPP95 and DPP90) and SWCNTs, leading to high PF values of up to 711.1 μW m^{-1} K^{-2}. Finally, the flexible TEGs consisting of a four-leg *p*-type DPP95/SWCNT nanocomposite were fabricated, which showed a maximum power output of 20.4 μW m^{-2} when the temperature difference (ΔT) was set to 29.3 K.

EXPERIMENTAL SECTION

Materials. The conjugated polymer samples, including DPP100, DPP90, DPP95, DPP90, DPP50, DPP30, DPP10, DPP5, and DPP0, were prepared using previously established synthetic protocols.[59] Tuball SWCNTs, obtained from OCSiAl, with a radius below 2 nm and a length greater than 5 μm and a purity of approximately 80% were used in this study.

Preparation of Random Conjugated Copolymers/SWCNT Nanocomposite Solution. To prepare the nanocomposite solutions, 1.5 mg of each conjugated copolymer was placed in individual 4 mL vials. Anhydrous 1,4-dichlorobenzene (DCB) was added to the vials to obtain predispersed solutions with a uniform concentration of 0.5 mg mL^{-1} for all samples. The solutions were heated overnight at 75 °C on a hot plate to ensure the complete dissolution of the polymers before ball milling. Next, 1.5 mg of SWCNTs was added to each vial at a 1:1 weight ratio with respect to the polymers. The resultant mixtures were dispersed by using a ball mill (Restch MM440) at 30 Hz for 20 min to obtain random conjugated copolymer/SWCNT nanocomposite solutions with well-dispersed SWCNTs.

Fabrication and Measurement of *p*-Type Nanocomposite Thermoelectrics. To prepare the random conjugated copolymers/SWCNT nanocomposite films, we spin-coated the nanocomposite solutions onto glass substrates at 1000 rpm for 10 s. The films were then vacuum-treated overnight at 50 °C to evaporate any residual solvents and subsequently annealed at 190 °C in an N_2-filled glovebox. Before spin-coating, the glass substrates were sequentially cleaned with deionized water, acetone, and isopropyl alcohol and then blown dry with N_2. The thickness of the resulting random conjugated copolymer/SWCNT nanocomposite films spanned the range of 60−100 nm. The S and σ of the nanocomposite samples were measured using a thermoelectric tester ZEM-3 (Advance Riko) at a temperature of 323 K, in the in-plane direction, where the charge transport channel is parallel to the sample surface. The experiment was conducted under a helium atmosphere to minimize any interference from oxygen or other gases.

Fabrication and Measurement of Flexible Nanocomposite Thermoelectric Generators. The flexible TEGs were fabricated through a series of manufacturing steps according to an established procedure. A DPP95/SWCNT nanocomposite solution was employed, and a blade-coating technique was utilized to deposit the solution onto a poly(ethylene terephthalate) (PET) substrate. A shadow mask was employed to define the desired dimensions and shape of each TEG. The TEGs were designed with four rectangular thermoelectric legs with 0.5 and 1.5 cm in length. These legs were interconnected in series through the thermal evaporation of silver. To achieve the desired thickness of 2−3 μm, the blade-coating and vacuum annealing processes were iterated ten times, ensuring the appropriate layer thickness and structural integrity of the TEGs. A thorough evaluation of the TEG performance was conducted using a customized measurement system, which adhered to the standard environmental conditions. To generate the necessary ΔT, a water-cooling system was employed to control the temperatures at both the heat source and the heat sink. The heat sink temperature was meticulously maintained at a constant 298 K, while the temperature of the heat source was systematically adjusted to establish varying ΔT. For precise monitoring of the temperature of TEGs, a *K*-type thermocouple was affixed to their surfaces. The temperature measurements were acquired by using the Keithley DAQ 6510 multimeter system, ensuring accurate and reliable data collection. The output voltage and current of the TEGs were measured by using copper wires connected to copper probes. These measurements were recorded with the aid of a Keithley 2182A nanovoltmeter and a Keithley 2400 sourcemeter, respectively.

RESULTS AND DISCUSSION

Polymer Characterization. DPP/IID-based random conjugated copolymers are reported to have outstanding charge transport properties due to their monomer similarity and high crystallinity. These polymers were prepared with a high molecular weight (M_n) spanning the range of 50−90 kDa and demonstrated good solubility in organic solvents. This study aims to investigate the effect of different ratios of DPP/IID units in a series of random conjugated copolymers and their SWCNT nanocomposites on thermoelectric properties. The nanocomposite solutions of random conjugated copolymers and SWCNTs were prepared by dispersing the polymers and SWCNTs in dichlorobenzene (DCB). Figure 1b illustrates a relative energy diagram of the DPP/IID-based random conjugated copolymers and SWCNTs, revealing that the highest occupied molecular orbitals (HOMOs) of all random conjugated copolymers (approximately −5.20 to −5.39 eV) are positioned higher than that of pristine SWCNTs (−5.10 eV). The elevated HOMO levels of the conjugated polymers facilitate efficient charge transport across the polymer/SWCNT junctions, primarily due to the successful charge separation.[60,61] This effect selectively scatters carriers with a lower thermal energy while permitting those with higher energy to traverse the interface. Consequently, this phenomenon leads to an increase in the average energy of the carriers and enhances the S values of the thermoelectric materials.

Optical Spectroscopic Analysis. Figures 2, S2 and S9 display the UV−vis absorption spectra of the random conjugated copolymers and their SWCNT nanocomposites in the solution state. The absorption maximum (λ_{max}) of DPP100 (Figure 2a) was observed at 692 nm with a prominent shoulder at 778 nm. Similarly, for DPP0 (Figure 2d), the λ_{max} value occurred at 641 nm, accompanied by a strong shoulder at 704 nm. These spectral features indicate the presence of a highly conjugated system with a strong D−A interaction

https://doi.org/10.1021/acsami.3c11792
ACS Appl. Mater. Interfaces 2023, 15, 56116−56126

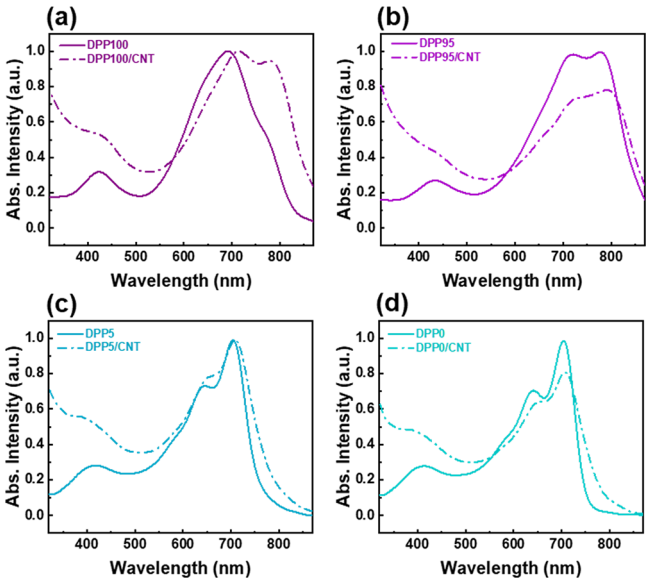

Figure 2. Normalized UV−vis absorption for the diluted solutions containing random conjugated copolymers and their SWCNT nanocomposites: (a) DPP100 and DPP100/SWCNT, (b) DPP95 and DPP95/SWCNT, (c) DPP5 and DPP5/SWCNT, and (d) DPP0 and DPP0/SWCNT.

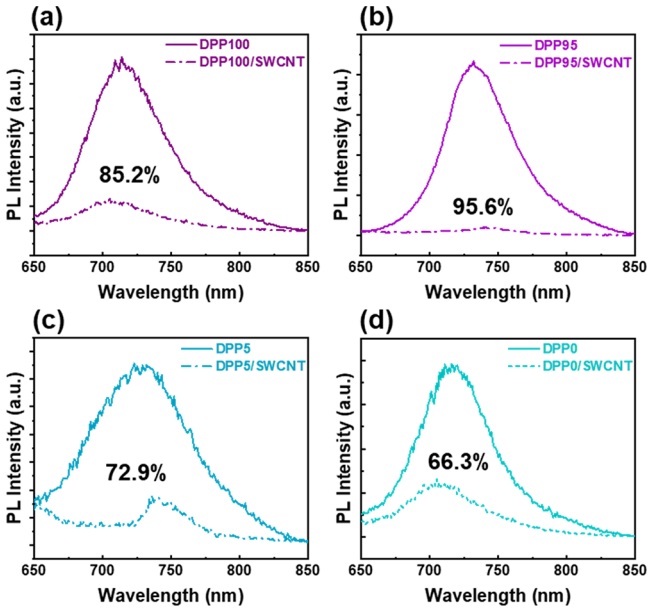

Figure 3. PL spectra for the diluted solutions containing random conjugated copolymers and their SWCNT nanocomposites: (a) DPP100 and DPP100/SWCNT, (b) DPP95 and DPP95/SWCNT, (c) DPP5 and DPP5/SWCNT, and (d) DPP0 and DPP0/SWCNT.

between the conjugated moieties. These two vibrational peaks (0−0 and 0−1) between 600 and 800 nm are attributed to the intermolecular vibrational coupling between the donor and acceptor moieties, where the absorption band across 400−500 nm originates from the $\pi-\pi^*$ transition. Upon addition of SWCNTs, the absorption peaks of the conjugated polymers were observed to red-shift by approximately 5−20 nm in the nanocomposite solutions, indicating the formation of interactions between the interface of random conjugated copolymers and the SWCNTs.[62] Furthermore, the nanocomposites exhibit a graphitic absorption feature, characterized by a π-electron plasmonic signal observed around 300 nm. This feature is attributed to the strong interaction occurring between the random conjugated copolymers and the surface of the SWCNTs.[63] It can be inferred that random conjugated copolymers with lower IID content, such as DPP100/SWCNT, DPP90/SWCNT, DPP95/SWCNT, and DPP50/SWCNT, exhibit more strongly red-shifted absorption spectra than those with higher IID content, such as DPP30/SWCNT, DPP10/SWCNT, DPP5/SWCNT, and DPP0/SWCNT, thereby indicating stronger intramolecular interactions of the conjugated polymers. In contrast, the random conjugated copolymers with a high IID content tend to form self-aggregates in the solution state, thereby confining their ability to interact with SWCNTs. These results imply that random conjugated copolymers with lower IID content are more likely to wrap around the SWCNTs via interactions and change their conformations to a more planar structure as they attach along the SWCNT surfaces.

The interactions between random conjugated copolymers and SWCNTs were further analyzed by examining their photoluminescence (PL) spectra in solution (Figures 3 and S3). PL quenching is observed due to the energy transfer from photoexcited electrons in the random conjugated copolymers to SWCNTs, indicating the extent and strength of the interaction between the two components. Strong interactions facilitate many polymer chains to wrap around the SWCNTs. Figure 3 presents the PL spectra of random conjugated copolymers and their corresponding nanocomposites in DCB, with each sample excited at the wavelength of maximum absorbance in the UV−vis spectrum. The PL quenching efficiency (PLQE) was calculated as PLQE (%) = $(I_0 - I/I_0) \times 100$, where I_0 and I are the peak intensity of the random conjugated copolymers and the corresponding random conjugated copolymer/SWCNT nanocomposites. The results indicate that the random conjugated copolymer/SWCNT nanocomposites with a lower IID content exhibited stronger PL quenching efficiency in comparison to those with a higher IID content. For instance, the DPP100/SWCNT, DPP95/SWCNT, DPP90/SWCNT, and DPP50/SWCNT nanocomposites show PLQE values of 85, 96, 91, and 92%, respectively, while the DPP30/SWCNT, DPP10/SWCNT, DPP5/SWCNT, and DPP0/SWCNT nanocomposites exhibit slightly lower PLQE values of 85, 77, 73, and 66%, respectively. The higher PLQE value observed in the DPP95/SWCNT nanocomposite can be attributed to efficient charge separation from the polymer to the SWCNTs. This suggests a stronger interaction between these two components, wherein a greater amount of the DPP95 polymer becomes wrapped around the SWCNT surfaces.

Figures 4 and S4 show the Raman spectra of pristine random conjugated copolymers and their nanocomposite films of random conjugated copolymer/SWCNTs. The G band of SWCNTs appears at 1593 cm^{-1}, which corresponds to the in-plane vibrations of sp^2-hybridized carbon atoms and the graphite stretching mode.[64] Interestingly, all of the nanocomposite films show low D bands and high G/D band ratios, indicating that the introduction of polymers does not result in structural defects. This suggests that the random conjugated copolymer/SWCNT nanocomposites are structurally stable, which is an important factor for thermoelectric applications. The pristine conjugated polymer films exhibit distinct peaks at approximately 1366 and 1420 cm^{-1}, corresponding to the intraunit C−C and C−N stretches involving the DPP unit.

https://doi.org/10.1021/acsami.3c11792
ACS Appl. Mater. Interfaces 2023, 15, 56116−56126

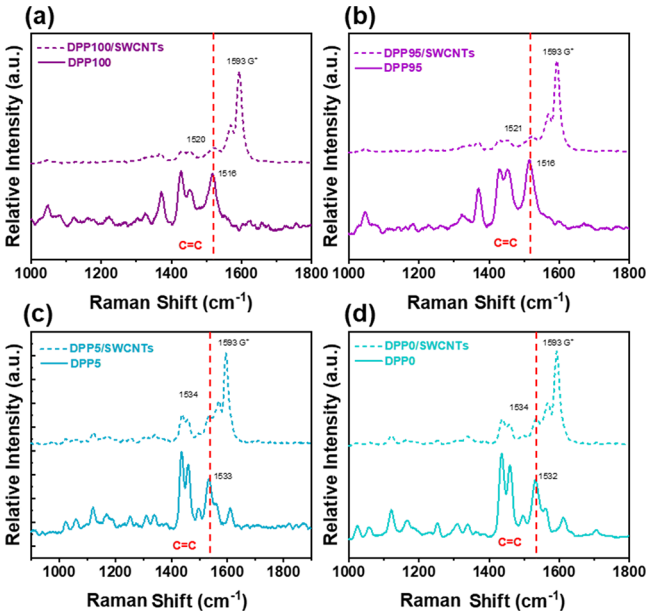

Figure 4. Raman spectra for the random conjugated copolymers and their SWCNT nanocomposite films: (a) DPP100 and DPP100/SWCNT, (b) DPP95 and DPP95/SWCNT, (c) DPP5 and DPP5/SWCNT, and (d) DPP0 and DPP0/SWCNT (the wavelength of the laser used was 532 nm).

Additionally, a peak at around 1516 cm^{-1} for DPP-rich random conjugated copolymers and 1532 cm^{-1} for IID-rich random conjugated copolymers is attributed to the C=C symmetric stretching of the intraunit backbone.[65,66] In the Raman spectra of the random conjugated copolymer/SWCNT nanocomposite films, the intensity of the characteristic peaks of the random conjugated copolymers gradually diminishes with the introduction of SWCNTs, while the peaks representing the symmetric C=C stretching of the intraunit backbone of all random conjugated copolymer/SWCNT nanocomposites exhibit a slight blue-shift. This observation signifies the presence of strong $\pi-\pi$ interactions between the random conjugated copolymers and SWCNTs. Furthermore, the DPP95/SWCNT nanocomposite exhibiting the highest PLQE demonstrates a significant Raman shift of 4 cm^{-1} compared to other nanocomposites studied. This shift indicates that the interactions between DPP95 and SWCNTs are stronger in this particular nanocomposite than in other random conjugated copolymers examined in this study.

Morphological and Microstructural Analysis. To investigate the surface morphologies, the conjugated polymer/SWCNT nanocomposite films were characterized using field scanning electron microscopy (SEM), transmission electron microscopy (TEM), and atomic force microscopy (AFM), as shown in Figures 5 and S5–S7. The surfaces maintain the fiber-like structures of SWCNT bundles with a diameter range of 10–30 nm. The conjugated polymers are tightly attached on the surface of the SWCNTs through the strong $\pi-\pi$ interactions, which can be clearly observed in the SEM images (Figures 5a–d and S5). The fibers overlapped with each other, forming interconnected networks that create electrical pathways in the conjugated polymer/SWCNT nanocomposite films. The DPP100/SWCNT, DPP5/SWCNT, and DPP0/SWCNT films showed a higher occurrence of defects in the nanocomposite, including interfaces, junctions, and nanopores. These defects could potentially contribute to the higher S observed in these nanocomposites.[67–69] In comparison to the DPP100/SWCNT, DPP5/SWCNT, and DPP0/SWCNT films, the DPP95/SWCNT film shows a more uniform morphology throughout the entire surface area along with a smaller fiber

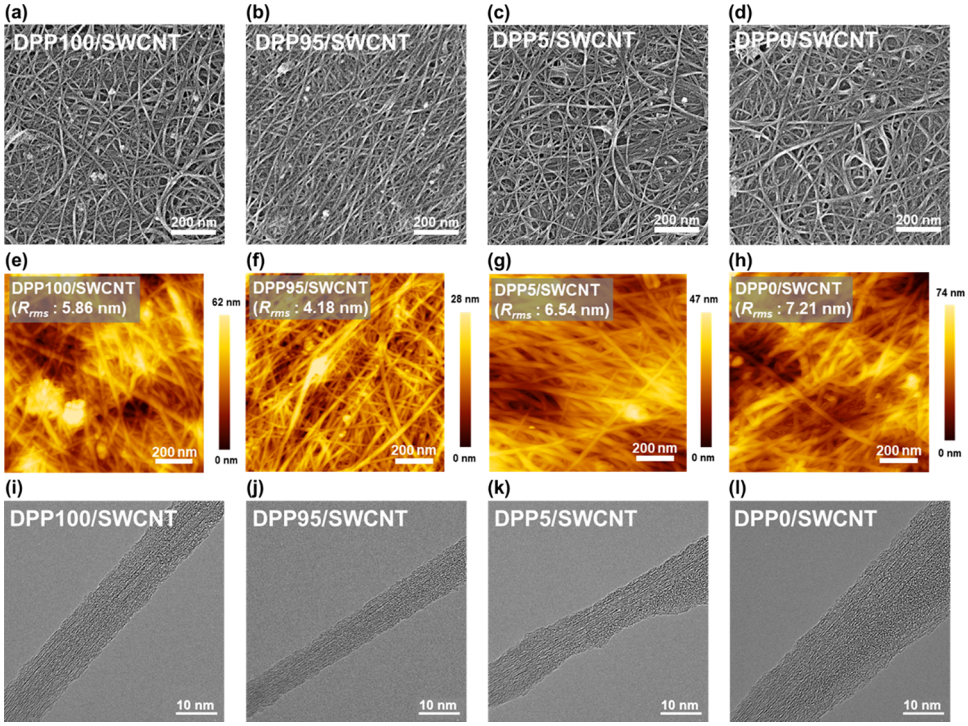

Figure 5. Surface morphologies of the random conjugated copolymer/SWCNT nanocomposite films: (a–d) SEM, (e–h) AFM, and (i–l) TEM images.

https://doi.org/10.1021/acsami.3c11792
ACS Appl. Mater. Interfaces 2023, 15, 56116–56126

diameter (10 nm), which is attributed to a better dispersion of SWCNTs in the solution facilitated by DPP95. The conjugated polymers with lower IID content, such as DPP95 and DPP90, interact more strongly with SWCNTs such that they can firmly and evenly wrap on the SWCNT surface and provide a better colloidal stability in the solvent, as evidenced by the PL and Raman results (Figures 3 and 4).

The surface morphologies of the conjugated polymer/SWCNT nanocomposite films were further examined using an atomic force microscope. The height images are shown in Figures 5e–h and S7 where fiber-like structures are clearly seen, identical to the SEM images (Figure 5a–d). The root-mean-square surface roughness (R_{rms}) was estimated from the AFM images and decreased with the fiber diameter in the following order: DPP0/SWCNT (7.21 nm) > DPP5/SWCNT (6.54 nm) > DPP10/SWCNT (6.22 nm) > DPP100/SWCNT (5.86 nm) > DPP30/SWCNT (5.51 nm) > DPP50/SWCNT (4.91 nm) > DPP90/SWCNT (4.28 nm) > DPP95/SWCNT (4.18 nm), as summarized in Figure S4. DPP90 and DPP95 of stronger interactions with the SWCNT also lead to a smoother film surface.

The isolated SWCNT bundles wrapped by the polymers were probed by TEM, as shown in Figures 5i–l and S6, which were prepared on copper grids from the 1000 times diluted solutions. The diameters of the SWCNT bundles range from 8 to 15 nm. As the IID content increases, the wrapping of the polymers on SWCNTs is less uniform, causing the uneven diameter of the isolated SWCNT bundle. This explains the less regular distribution of the SWCNT bundles in the DPP50/SWCNT, DPP30/SWCNT, DPP10/SWCNT, and DPP5/SWCNT films (Figure S6b,d,k), which consequently leads to a decrease in the contact area between fibers and a decline in the potential electrical pathways. In contrast, both DPP95 and DPP90 with low IID content strongly adhere to the surfaces of SWCNTs through the $\pi-\pi$ interactions, resulting in a smooth and continuous polymer coverage on the SWCNT surfaces. The stronger interactions between DPP95/DPP90 and SWCNTs protect SWCNTs from aggregation, thereby giving rise to thinner SWCNT bundles that form a network of a more efficient electrical conduction pathway.

Grazing-incidence wide-angle X-ray scattering (GIWAXS) was employed to analyze the microstructures of the conjugated copolymer/SWCNT nanocomposites and investigate the interplay between the conjugated polymers and SWCNTs. As shown in Figures 6 and S8, the polymers without SWCNT form highly regular lamellar structures arranged in an edge-on manner in the films, evidenced by the high-order diffraction peaks in the out-of-phase direction. Upon the incorporation of SWCNTs, the diffractions from the lamellae disappear, and only a diffraction ring at $q \approx 2.1$ Å^{-1} can be seen, which is characteristic of the SWCNTs. This indicates that the conjugated polymers in these nanocomposites are unable to stack into long-ranged lamellae in the presence of SWCNTs. In other words, the conjugated polymers and SWCNTs interplay in a molecular level, and the strong interactions with SWCNTs hinder the regular packing of the conjugated polymers wrapped on the SWCNTs. It has been previously reported that a high fraction of SWCNTs impedes the formation of crystalline regions within the conjugated polymers.[47]

Thermoelectric Properties of Nanocomposite Thin Films. Figure 7 and Table 2 depict the variations in the S, σ, and PF of the random conjugated copolymer/SWCNT nanocomposite films at a mass ratio of 1/1 and a temperature

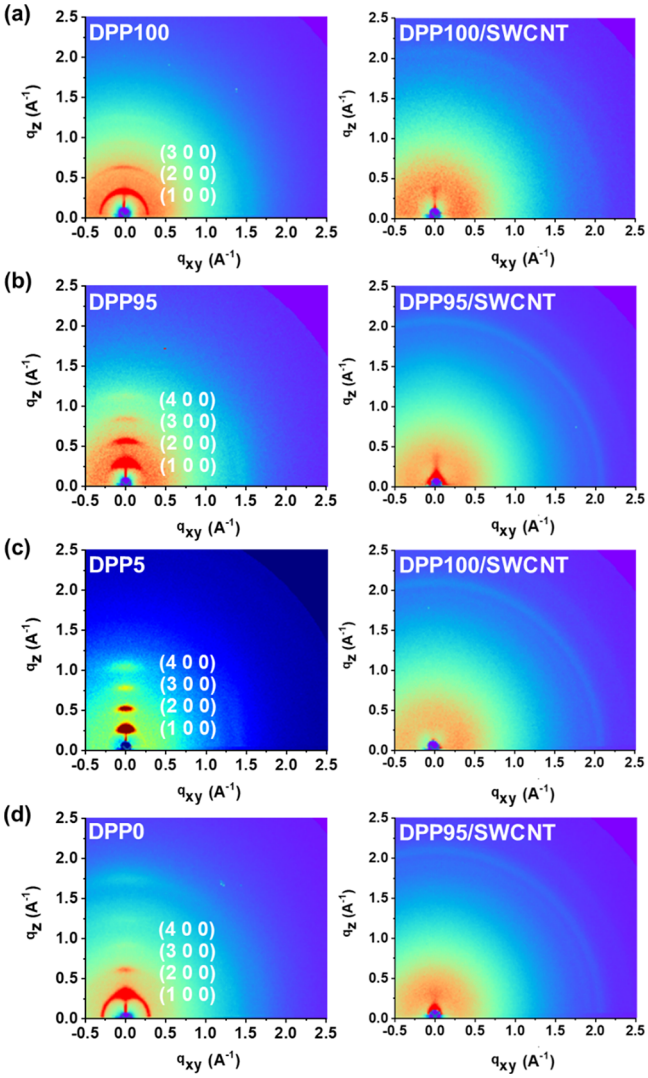

Figure 6. GIWAXS patterns of the random conjugated copolymers and their SWCNT films: (a) DPP100 and DPP100/SWCNT, (b) DPP95 and DPP95/SWCNT, (c) DPP5 and DPP5/SWCNT, and (d) DPP0 and DPP0/SWCNT.

of 323 K. All the random conjugated copolymer/SWCNT nanocomposites demonstrate p-type transport characteristics, confirmed by their positive S value, with holes being the primary charge carrier transported under the ΔT. The S values of the different random conjugated copolymer/SWCNT nanocomposite films are shown in Figure 7a. The enhanced carrier energy scattering between the energy barriers of random conjugated copolymers and SWCNTs enables the DPP5/SWCNT nanocomposite to achieve a high peak S value of approximately 65.8 μV K^{-1}. This achievement is attributed to the effective creation of the highest energy barrier against SWCNTs by DPP5, thereby selectively removing accumulated holes with low energy. As a result, the average energy of the remaining accumulated holes is increased, leading to an overall enhancement in the S.[70] Moreover, the defects present in the DPP5/SWCNT nanocomposite may have contributed to the higher S compared to that in other nanocomposites. Figure 7b plots the σ values of the random conjugated copolymer/SWCNT nanocomposite films, with DPP95/SWCNTs achieving the highest σ of 1553.8 S cm^{-1}. This high performance can be attributed to the stronger $\pi-\pi$ interactions between DPP95

https://doi.org/10.1021/acsami.3c11792
ACS Appl. Mater. Interfaces 2023, 15, 56116–56126

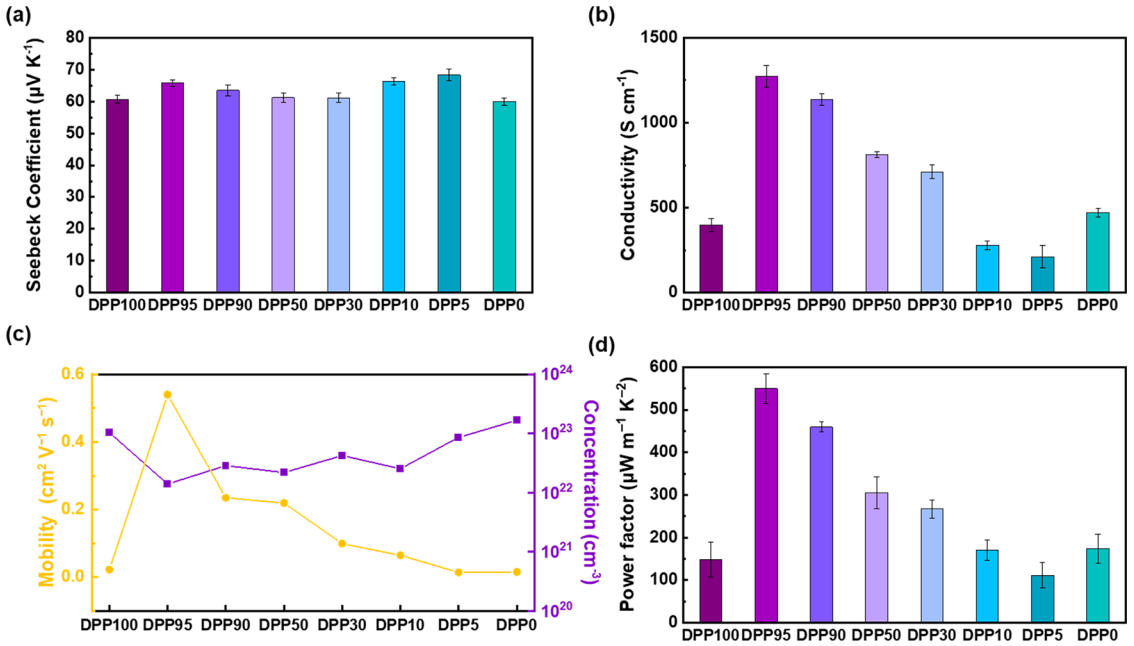

Figure 7. Thermoelectric properties of random conjugated copolymer/SWCNT nanocomposite thin films with an optimized mass ratio of 1:1: (a) S, (b) σ, (c) μ and n, and (d) PF.

Table 2. Thermoelectric Parameters of the Conjugated Polymer/SWCNT Nanocomposites Studied

nanocomposite	σ (σ_{max}) [S cm^{-1}]	S (S_{max}) [μV K^{-1}]	PF (PF$_{max}$) [μW m^{-1} K^{-2}]
DPP100/SWCNT	397.7 ± 37.8 (463.8)	60.7 ± 1.3 (63.9)	147.5 ± 41.0 (172.2)
DPP95/SWCNT	1274.2 ± 63.2 (1689.7)	65.8 ± 1.0 (66.0)	549.8 ± 70.4 (711.1)
DPP90/SWCNT	1135.8 ± 33.6 (1178.9)	63.5 ± 1.7 (65.2)	459.2 ± 11.9 (473.3)
DPP50/SWCNT	811.4 ± 18.2 (830.8)	61.2 ± 1.4 (62.4)	305.0 ± 37.4 (342.1)
DPP30/SWCNT	712.2 ± 41.3 (778.9)	61.1 ± 1.5 (62.8)	266.7 ± 20.8 (305.2)
DPP10/SWCNT	278.7 ± 24.8 (321.7)	66.3 ± 1.2 (67.3)	170.7 ± 24.0 (212.1)
DPP5/SWCNT	212.2 ± 67.2 (339.6)	68.3 ± 1.8 (73.2)	111.4 ± 29.3 (158.1)
DPP0/SWCNT	470.9 ± 23.6 (507.7)	59.9 ± 1.1 (61.6)	173.8 ± 33.5 (213.7)

and SWCNTs, resulting in smaller SWCNT bundles in comparison to other random conjugated copolymers. Therefore, the tight binding between the wrapped DPP95 and the debundled SWCNTs contributes to a larger number of SWCNT junctions and a lower contact resistance, resulting in a higher σ in the nanocomposite film. The differences in σ between the nanocomposites depend on how efficiently each conjugated polymer mediates charge transport between adjacent CNTs. Therefore, we perform Hall effect measurements to quantify the carrier mobility (μ) in each nanocomposite film (Figure 7c). The differences between n of all of the nanocomposites are small because of their identical compositions (conjugated polymer: SWCNT = 1:1 by weight); however, the μ of the DPP95/SWCNT nanocomposite is estimated to be 0.53 cm^2 V^{-1} s^{-1}, which is much higher than that of other random conjugated copolymer/SWCNT nanocomposites. Based on the relation of ($\sigma = n\ e\ \mu$, where e is the elementary charge), a high σ in DPP95/SWCNT may be attributed to the efficient charge transport properties between DPP95 and SWCNTs, which is strengthened by strong $\pi-\pi$ interfacial interactions. Next, the calculated PF ($= \sigma S^2$) in Figure 7d, which is derived from the S and σ, exhibits a trend similar to that of σ for all nanocomposites. The σ predominantly influences the thermoelectric properties of the nanocomposites, outweighing the slight decrease in S. It is noteworthy that the DPP95/SWCNT nanocomposite exhibits the highest PF value of 711 μW m^{-1} K^{-2} reported thus far among the D−A conjugated polymer/SWCNT nanocomposites, as shown in Figure S1. This outperformance indicates that the DPP95/SWCNT nanocomposite has a favorable combination of high σ and S, resulting in improved thermoelectric performance compared to those of the other nanocomposites studied. As illustrated in Figure S10, the DPP95/SWCNT nanocomposite showcases notable thermal stability, efficiently operating over a temperature spectrum ranging from 293 to 373 K. Upon practical deployment and meticulous examination, it has been discerned that the electrical conductivities of these composite materials sustain a consistent performance with negligible degradation across numerous heating and cooling cycles. This inherent thermal resilience significantly augments the enduring efficacy of the composites in real-world applications, where temperature fluctuations are a common occurrence.

Flexible DPP95/SWCNT Nanocomposite Thermoelectric Generators. After selecting the optimized performance of the DPP95/SWCNT nanocomposite for further investigation, planar-type flexible TEGs were fabricated by blade-coating a nanocomposite solution onto a poly(ethylene terephthalate) (PET) substrate using a shadow mask. The TEGs consisted of four rectangular thermoelectric legs with a 0.5 cm width and a 1.5 cm length and were electrically connected in series through the thermal evaporation of silver. To achieve a thick film with a thickness of 2−3 μm, the blade-coating and vacuum annealing processes were repeated ten times. The connected geometric structure of the thermoelectric legs in the TEGs is illustrated in

https://doi.org/10.1021/acsami.3c11792
ACS Appl. Mater. Interfaces 2023, 15, 56116−56126

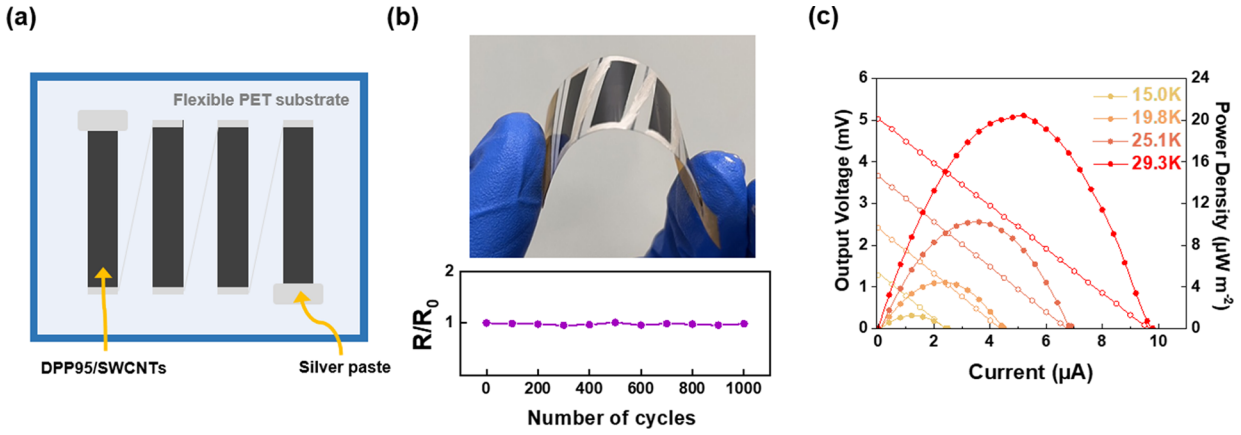

Figure 8. Flexible TEGs utilizing interconnected DPP95/SWCNT nanocomposite films as the thermoelectric legs. (a) Schematic representation of the TEGs consisting of four *p*-type legs. (b) R/R_0 as a function of bending cycles for flexible TEGs, where R_0 is the resistance at the original state (bending radius of 2.5 cm). (c) Output voltage and power density versus current curves of the TEGs at different ΔT.

Figure 7a, and a photograph of the completed flexible TEGs is shown in Figure 7b.

To evaluate the performance of the TEGs under environmental conditions, a specially designed measurement system was utilized. This system included a water-cooling setup that allowed for precise control of ΔT across the generator. The heat source and heat sink were both equipped with water-cooling systems to maintain stable and controlled temperature conditions. By adjustment of the water flow and temperature, the desired ΔT could be achieved and maintained during the measurements. This controlled setup ensured accurate and reliable evaluation of the TEG performance under realistic operating conditions. The output voltage and output power density were measured under steady-state ΔT values of 15.0, 19.8, 25.1, and 29.3 K. These measurements were plotted against the output current, as depicted in Figure 8c. The output voltage versus current density exhibited stability and linearity at each tested temperature, with both the output voltage and current increasing proportionally with an increase in ΔT. A highest output voltage of 5.03 mV and an output power density of 20.4 μW m^{-2} were achieved with a ΔT of 29.3 K. However, it is worth noting that the achieved *S* value of approximately 45 μV K^{-1} from the TEGs corresponded to only about 70% of the value obtained from a single thermoelectric cell. This discrepancy may be attributed to measurement errors, additional internal resistance caused by the electrical connections between the thermoelectric legs, and film thickness variations. Indeed, this research demonstrates the potential application of the prototype TEG by effectively manipulating the controllable energy levels of random conjugated copolymers and enhancing their interaction with SWCNTs. The TEGs show promising performance in harnessing and using low-grade waste heat. The ability to convert waste heat into electricity using this approach has significant implications for energy harvesting and sustainability. It opens up possibilities for the efficient utilization of previously untapped energy sources and contributes to the development of more environmentally friendly and energy-efficient technologies.

CONCLUSIONS

Through our investigation into the thermoelectric properties of polymer/SWCNT nanocomposites using eight DPP/IID-based random conjugated copolymers, we have discovered that tuning the energy levels can effectively manipulate the *S* value. Among all of the nanocomposites tested, DPP5/SWCNT exhibits a slightly higher *S* due to the presence of the largest energy barriers against SWCNTs and more defects present in the nanocomposite. Our spectroscopic and morphological analyses have revealed that the π-electron delocalization in the donor−acceptor conjugated polymer backbone facilitates strong interactions between the polymers and SWCNTs. In particular, DPP95 with a low IID content exhibits efficient debundling of SWCNTs by establishing a strong interaction between conjugated polymers and SWCNTs. This interaction leads to significant enhancements in the dispersion and σ. As a result, the DPP95/SWCNT nanocomposites demonstrate superior thermoelectric performance, exhibiting the highest PF of 711.1 μW m^{-1} K^{-2} based on *S* of 64.8 μV K^{-1} and σ of 1689.7 S cm^{-1}. Furthermore, we successfully constructed flexible TEGs using four-leg *p*-type DPP95/SWCNT nanocomposite films. These TEGs generate a maximum output voltage of 5.03 mV and an output power of 20.4 μW m^{-2} at a ΔT of 29.3 K. Our study highlights the potential of developing TEG devices for effectively harnessing low-grade waste heat by manipulating the energy levels of random conjugated copolymers with SWCNTs and improving their thermoelectric properties.

ASSOCIATED CONTENT

Supporting Information

The Supporting Information is available free of charge at https://pubs.acs.org/doi/10.1021/acsami.3c11792.

Instrumentation, UV−vis spectra, PL spectra, Raman spectra, TEM images, SEM images, AFM images, and GIWAXS patterns (PDF)

AUTHOR INFORMATION

Corresponding Authors

Yan-Cheng Lin − *Department of Chemical Engineering, National Cheng Kung University, Tainan 70101, Taiwan; Advanced Research Center of Green Materials Science and Technology, National Taiwan University, Taipei 10617, Taiwan;* orcid.org/0000-0002-2914-6762; Email: ycl@gs.ncku.edu.tw

Cheng-Liang Liu − *Department of Materials Science and Engineering and Advanced Research Center of Green*

https://doi.org/10.1021/acsami.3c11792
ACS Appl. Mater. Interfaces 2023, 15, 56116−56126

Materials Science and Technology, National Taiwan University, Taipei 10617, Taiwan; orcid.org/0000-0002-8778-5386; Email: liucl@ntu.edu.tw

Authors

Kuan-Chieh Wang − *Department of Materials Science and Engineering, National Taiwan University, Taipei 10617, Taiwan*

Po-Shen Lin − *Department of Materials Science and Engineering, National Taiwan University, Taipei 10617, Taiwan*

Shih-Huang Tung − *Institute of Polymer Science and Engineering, National Taiwan University, Taipei 10617, Taiwan;* orcid.org/0000-0002-6787-4955

Wen-Chang Chen − *Advanced Research Center of Green Materials Science and Technology and Department of Chemical Engineering, National Taiwan University, Taipei 10617, Taiwan;* orcid.org/0000-0003-3170-7220

Complete contact information is available at: https://pubs.acs.org/10.1021/acsami.3c11792

Author Contributions

#K.-C.W., P.-S.L., and Y.-C.L. contributed equally to this work.

Notes

The authors declare no competing financial interest.

■ ACKNOWLEDGMENTS

The authors acknowledge the financial support from the 2030 Cross-Generation Young Scholars Program by the National Science and Technology Council (NSTC) in Taiwan under grant 111-2628-E-002-014 and 112-2628-E-002-013, Academic Research-Career Development Project (Sprout Research Projects) by National Taiwan University (NTU112L7856), and Advanced Research Center for Green Materials Science and Technology from the Featured Area Research Center Program within the framework of the Higher Education Sprout Project by the Ministry of Education (112L9006). The authors thank Beamline TLS 17A1 and TPS 25A at the National Synchrotron Radiation Research Center (NSRRC) of Taiwan for providing beamtime.

■ REFERENCES

(1) Hashemi, S. A.; Ramakrishna, S.; Aberle, A. G. Recent Progress in Flexible−wearable Solar Cells for Self-powered Electronic Devices. *Energy Environ. Sci.* **2020**, *13* (3), 685−743.

(2) Guan, X.; Xu, B.; Gong, J. Hierarchically Architected Polydopamine Modified $BaTiO_3$@P(VDF-TrFE) Nanocomposite Fiber Mats for Flexible Piezoelectric Nanogenerators and Self-powered Sensors. *Nano Energy* **2020**, *70*, No. 104516.

(3) Wang, Y.; Yang, L.; Shi, X.-L.; Shi, X.; Chen, L.; Dargusch, M. S.; Zou, J.; Chen, Z.-G. Flexible Thermoelectric Materials and Generators: Challenges and Innovations. *Adv. Mater.* **2019**, *31* (29), No. 1807916.

(4) Ding, J.; Zhao, W.; Jin, W.; Di, C.-A.; Zhu, D. Advanced Thermoelectric Materials for Flexible Cooling Application. *Adv. Funct. Mater.* **2021**, *31* (20), No. 2010695.

(5) Deng, L.; Liu, Y.; Zhang, Y.; Wang, S.; Gao, P. Organic Thermoelectric Materials: Niche Harvester of Thermal Energy. *Adv. Funct. Mater.* **2023**, *33* (3), No. 2210770.

(6) Massetti, M.; Jiao, F.; Ferguson, A. J.; Zhao, D.; Wijeratne, K.; Würger, A.; Blackburn, J. L.; Crispin, X.; Fabiano, S. Unconventional Thermoelectric Materials for Energy Harvesting and Sensing Applications. *Chem. Rev.* **2021**, *121* (20), 12465−12547.

(7) Bao, Y.; Sun, Y.; Jiao, F.; Hu, W. Recent Advances in Multicomponent Organic Composite Thermoelectric Materials. *Adv. Electron. Mater.* **2023**, *9* (5), No. 2201310.

(8) Zhu, H.; Zhao, T.; Zhang, B.; An, Z.; Mao, S.; Wang, G.; Han, X.; Lu, X.; Zhang, J.; Zhou, X. Entropy Engineered Cubic n-Type $AgBiSe_2$ Alloy with High Thermoelectric Performance in Fully Extended Operating Temperature Range. *Adv. Energy Mater.* **2021**, *11* (5), No. 2003304.

(9) Jiang, B.; Yu, Y.; Cui, J.; Liu, X.; Xie, L.; Liao, J.; Zhang, Q.; Huang, Y.; Ning, S.; Jia, B.; et al. High-entropy-stabilized Chalcogenides with High Thermoelectric Performance. *Science* **2021**, *371* (6531), 830−834.

(10) Raja, V.; Hu, Z.; Chen, G. Progress in Poly(2,5-bis(3-alkylthiophen-2-yl)thieno[3,2-b]thiophene) Composites for Thermoelectric Application. *Compos. Commun.* **2021**, *27*, No. 100886.

(11) Suh, E. H.; Jeong, Y. J.; Oh, J. G.; Lee, K.; Jung, J.; Kang, Y. S.; Jang, J. Doping of Donor-Acceptor Polymers with Long Side Chains via Solution Mixing for Advancing Thermoelectric Properties. *Nano Energy* **2019**, *58*, 585−595.

(12) Wang, H.; Yu, C. Organic Thermoelectrics: Materials Preparation, Performance Optimization, and Device Integration. *Joule* **2019**, *3* (1), 53−80.

(13) Yusupov, K.; Vomiero, A. Polymer-based Low-temperature Thermoelectric Composites. *Adv. Funct. Mater.* **2020**, *30* (52), No. 2002015.

(14) Zhang, F.; Di, C.-A. Exploring Thermoelectric Materials from High Mobility Organic Semiconductors. *Chem. Mater.* **2020**, *32* (7), 2688−2702.

(15) Jia, Y.; Jiang, Q.; Sun, H.; Liu, P.; Hu, D.; Pei, Y.; Liu, W.; Crispin, X.; Fabiano, S.; Ma, Y.; et al. Wearable Thermoelectric Materials and Devices for Self-powered Electronic Systems. *Adv. Mater.* **2021**, *33* (42), No. 2102990.

(16) Zhang, L.; Shi, X.-L.; Yang, Y.-L.; Chen, Z.-G. Flexible Thermoelectric Materials and Devices: From Materials to Applications. *Mater. Today* **2021**, *46*, 62−108.

(17) Hao, Y.; He, X.; Wang, L.; Qin, X.; Chen, G.; Yu, J. Stretchable Thermoelectrics: Strategies, Performances, and Applications. *Adv. Funct. Mater.* **2022**, *32* (13), No. 2109790.

(18) Wang, J.; Liu, L.; Wu, F.; Liu, Z.; Fan, Z.; Chen, L.; Chen, Y. Recent Developments of n-Type Organic Thermoelectric Materials: Influence of Structure Modification on Molecule Arrangement and Solution Processing. *ChemSusChem* **2022**, *15* (4), No. e202102420.

(19) Zhou, D.; Zhang, H.; Zheng, H.; Xu, Z.; Xu, H.; Guo, H.; Li, P.; Tong, Y.; Hu, B.; Chen, L. Recent Advances and Prospects of Small Molecular Organic Thermoelectric Materials. *Small* **2022**, *18* (23), No. 2200679.

(20) Vijitha, I.; Jacob, N.; Raveendran, N.; Vijayakumar, C.; Deb, B. Simulation-aided Studies on the Superior Thermoelectric Performance of Printable PBDTT-FTTE/SWCNT Composites. *Mater. Today Energy* **2023**, *32*, No. 101233.

(21) Sung, D. H.; Kang, G.-H.; Kong, K.; Kim, M.; Park, H. W.; Park, Y.-B. Characterization of Thermoelectric Properties of Multifunctional Multiscale Composites and Fiber-reinforced Composites for Thermal Energy Harvesting. *Compos. B: Eng.* **2016**, *92*, 202−209.

(22) Li, J.; Wang, Z.; Sun, Z.; Xu, L.; Wong, W.-Y. Effect of the Linking Group on the Thermoelectric Properties of Poly(Schiff Base)s and Their Metallopolymers. *Chem.—Asian J.* **2021**, *16* (14), 1911−1917.

(23) Li, J.; Guo, Z.; Xu, L.; Wong, W.-Y. Synthesis of Bis-Terpyridine-Based Metallopolymers and the Thermoelectric Properties of Their Single Walled Carbon Nanotube Composites. *Molecules* **2021**, *26*, 2560 DOI: 10.1016/j.omtn.2021.05.018.

(24) Nonoguchi, Y. Recent Progress in Thermoelectric Materials Based on Single-wall Carbon Nanotubes. *Carbon* **2021**, *176*, 657.

(25) Liu, Y.; Villalva, D. R.; Sharma, A.; Haque, M. A.; Baran, D. Molecular Doping of a Naphthalene Diimide−Bithiophene Copolymer and SWCNTs for n-Type Thermoelectric Composites. *ACS Appl. Mater. Interfaces* **2021**, *13* (1), 411−418.

(26) Wang, Y.; Li, K.; Wang, J.; Dai, X.; Sun, X.; Chong, D.; Yan, J.; Zhang, L.; Wang, H. Green Biopolymer-CNT Films Exhibit High Thermoelectric Power Factor and Electrical Conductivity for Low Temperature Heat Energy Harvesting. *J. Mater. Chem. A* **2022**, *10* (48), 25740−25751.
(27) Zhang, Y.; Zhang, Q.; Chen, G. Carbon and Carbon Composites for Thermoelectric Applications. *Carbon Energy* **2020**, *2* (3), 408−436.
(28) Liang, J.; Cui, R.; Zhang, X.; Koumoto, K.; Wan, C. Polymer/Carbon Composites with Versatile Interfacial Interactions for High Performance Carbon-Based Thermoelectrics: Principles and Applications. *Adv. Funct. Mater.* **2023**, *33* (9), No. 2208813.
(29) Prunet, G.; Pawula, F.; Fleury, G.; Cloutet, E.; Robinson, A. J.; Hadziioannou, G.; Pakdel, A. A Review on Conductive Polymers and Their Hybrids for Flexible and Wearable Thermoelectric Applications. *Mater. Today Phys.* **2021**, *18*, No. 100402.
(30) Choi, J.; Jung, Y.; Yang, S. J.; Oh, J. Y.; Oh, J.; Jo, K.; Son, J. G.; Moon, S. E.; Park, C. R.; Kim, H. Flexible and Robust Thermoelectric Generators Based on All-Carbon Nanotube Yarn without Metal Electrodes. *ACS Nano* **2017**, *11* (8), 7608−7614.
(31) Zhou, H.; Chua, M. H.; Zhu, Q.; Xu, J. High-performance PEDOT:PSS-based Thermoelectric Composites. *Compos. Commun.* **2021**, *27*, No. 100877.
(32) Zhang, L.; Xia, B.; Shi, X.-L.; Liu, W.-D.; Yang, Y.; Hou, X.; Ye, X.; Suo, G.; Chen, Z.-G. Achieving High Thermoelectric Properties in PEDOT:PSS/SWCNTs Composite Films by a Combination of Dimethyl Sulfoxide Doping and $NaBH_4$ Dedoping. *Carbon* **2022**, *196*, 718−726.
(33) Wang, L.; Zhang, J.; Guo, Y.; Chen, X.; Jin, X.; Yang, Q.; Zhang, K.; Wang, S.; Qiu, Y. Fabrication of Core-shell Structured Poly(3,4-ethylenedioxythiophene)/Carbon Nanotube Hybrids with Enhanced Thermoelectric Power Factors. *Carbon* **2019**, *148*, 290−296.
(34) Chen, J.; Wang, L.; Gui, X.; Lin, Z.; Ke, X.; Hao, F.; Li, Y.; Jiang, Y.; Wu, Y.; Shi, X.; et al. Strong Anisotropy in Thermoelectric Properties of CNT/PANI Composites. *Carbon* **2017**, *114*, 1−7.
(35) Feng, L.; Wu, R.; Liu, C.; Lan, J.; Lin, Y.-H.; Yang, X. Facile Green Vacuum-Assisted Method for Polyaniline/SWCNT Hybrid Films with Enhanced Thermoelectric Performance by Interfacial Morphology Control. *ACS Appl. Energy Mater.* **2021**, *4* (4), 4081−4089.
(36) Wang, S.; Liu, F.; Gao, C.; Wan, T.; Wang, L.; Wang, L.; Wang, L. Enhancement of the Thermoelectric Property of Nanostructured Polyaniline/Carbon Nanotube Composites by Introducing Pyrrole Unit onto Polyaniline Backbone via a Sustainable Method. *Chem. Eng. J.* **2019**, *370*, 322−329.
(37) Lin, P.-S.; Inagaki, S.; Liu, J.-H.; Chen, M.-C.; Higashihara, T.; Liu, C.-L. The Role of Branched Alkylthio Side Chain on Dispersion and Thermoelectric Properties of Regioregular Polythiophene/Carbon Nanotubes Nanocomposites. *Chem. Eng. J.* **2023**, *458*, No. 141366.
(38) Tonga, M.; Wei, L.; Wilusz, E.; Korugic-Karasz, L.; Karasz, F. E.; Lahti, P. M. Solution-Fabrication Dependent Thermoelectric Behavior of Iodine-doped Regioregular and Regiorandom P3HT/Carbon Nanotube Composites. *Synth. Met.* **2018**, *239*, 51−58.
(39) Wang, L.; Pan, C.; Chen, Z.; Zhou, W.; Gao, C.; Wang, L. Enhanced Thermoelectric Performance of Conjugated Polymer/Single-Walled Carbon Nanotube Composites with Strong Stacking. *ACS Appl. Energy Mater.* **2018**, *1* (9), 5075−5082.
(40) Wan, T.; Yin, X.; Pan, C.; Liu, D.; Zhou, X.; Gao, C.; Wong, W.-Y.; Wang, L. Boosting the Adhesivity of π-Conjugated Polymers by Embedding Platinum Acetylides towards High-Performance Thermoelectric Composites. *Polymers* **2019**, *11* (4), 593.
(41) Kang, Y. H.; Lee, U.-H.; Jung, I. H.; Yoon, S. C.; Cho, S. Y. Enhanced Thermoelectric Performance of Conjugated Polymer/CNT Nanocomposites by Modulating the Potential Barrier Difference between Conjugated Polymer and CNT. *ACS Appl. Electron. Mater.* **2019**, *1* (7), 1282−1289.
(42) Chen, Z.; Liu, T.; Pan, C.; Tan, G. Enhanced Thermoelectric Performance of Indacenodithiophene-Benzothiadiazole Copolymer Containing Polar Side Chains and Single Wall Carbon Nanotubes Composites. *Polymers* **2020**, *12* (4), 848.
(43) Jung, J.; Suh, E. H.; Jeong, Y. J.; Yang, H. S.; Lee, T.; Jang, J. Efficient Debundling of Few-Walled Carbon Nanotubes by Wrapping with Donor-Acceptor Polymers for Improving Thermoelectric Properties. *ACS Appl. Mater. Interfaces* **2019**, *11* (50), 47330−47339.
(44) Chen, Z.; Lai, M.; Cai, L.; Zhou, W.; Xie, D.; Pan, C.; Qiu, Y. Boosting the Power Factor of Benzodithiophene Based Donor−Acceptor Copolymers/SWCNTs Composites through Doping. *Polymers* **2020**, *12* (7), 1447.
(45) Zhou, X.; Pan, C.; Liang, A.; Wang, L.; Wong, W.-Y. Thermoelectric Properties of Composite Films Prepared with Benzodithiophene Derivatives and Carbon Nanotubes. *Compos. Sci. Technol.* **2017**, *145*, 40−45.
(46) Zhou, H.; Li, X.; Gao, C.; Yang, F.; Ye, X.; Liu, Y.; Wang, L. The Ameliorative Thermoelectric Performance Induced by Heteroatom for Dithiophene Cyclopentadiene-based Polymers and Carbon Nanotubes Composite Films. *Compos. Sci. Technol.* **2021**, *201*, No. 108518.
(47) Kim, S. H.; Jeong, S.; Kim, D.; Son, C. Y.; Cho, K. Effects of Connecting Polymer Structure and Morphology at Inter-Tube Junctions on the Thermoelectric Properties of Conjugated Polymer/Carbon Nanotube Composites. *Adv. Electron. Mater.* **2023**, *9* (7), No. 2201293.
(48) Huang, H.; Chen, Z.; Chen, X.; Jin, J.; Huang, S.; Wang, D.; Wang, L.; Liu, D. Substrate Modification for High-Performance Thermoelectric Materials and Generators Based on Polymer and Carbon Nanotube Composite. *Adv. Mater. Interfaces* **2022**, *9* (23), No. 2201193.
(49) Goo, G.; Anoop, G.; Unithrattil, S.; Kim, W. S.; Lee, H. J.; Kim, H. B.; Jung, M.-H.; Park, J.; Ko, H. C.; Jo, J. Y. Proton-Irradiation Effects on the Thermoelectric Properties of Flexible Bi_2Te_3/PEDOT:PSS Composite Films. *Adv. Electron. Mater.* **2019**, *5* (4), No. 1800786.
(50) Kim, W. S.; Anoop, G.; Jeong, I.-S.; Lee, H. J.; Kim, H. B.; Kim, S. H.; Goo, G. W.; Lee, H.; Lee, H. J.; Kim, C.; et al. Feasible Tuning of Barrier Energy in PEDOT:PSS/Bi_2Te_3 Nanowires-based Thermoelectric Nanocomposite Thin Films through Polar Solvent Vapor Annealing. *Nano Energy* **2020**, *67*, No. 104207.
(51) Lee, H. J.; Anoop, G.; Lee, H. J.; Kim, C.; Park, J.-W.; Choi, J.; Kim, H.; Kim, Y.-J.; Lee, E.; Lee, S.-G.; et al. Enhanced Thermoelectric Performance of PEDOT:PSS/PANI−CSA Polymer Multilayer Structures. *Energy Environ. Sci.* **2016**, *9* (9), 2806−2811.
(52) Lee, H. M.; Anoop, G.; Lee, H. J.; Kim, W. S.; Jo, J. Y. Key Parameters for Enhancing the Thermoelectric Power Factor of PEDOT:PSS/PANI-CSA Multilayer Thin Films. *RSC Adv.* **2019**, *9* (21), 11595−11601.
(53) Liu, Z.; Chen, G. Advancing Flexible Thermoelectric Devices with Polymer Composites. *Adv. Mater. Technol.* **2020**, *5* (7), No. 2000049.
(54) Wang, Y.; Yang, X.; Pandolfo, A. G.; Ding, J.; Li, D. High-Rate and High-Volumetric Capacitance of Compact Graphene−Polyaniline Hydrogel Electrodes. *Adv. Energy Mater.* **2016**, *6* (11), 1600185.
(55) Liu, W. D.; Yu, Y.; Dargusch, M.; Liu, Q. F.; Chen, Z. G. Carbon Allotrope Hybrids Advance Thermoelectric Development and Applications. *Renew. Sust. Energy Rev.* **2021**, *141*, No. 110800.
(56) Wei, S.; Zhang, Y.; Lv, H.; Deng, L.; Chen, G. SWCNT Network Evolution of PEDOT:PSS/SWCNT Composites for Thermoelectric Application. *Chem. Eng. J.* **2022**, *428*, No. 131137.
(57) Liu, S.; Li, H.; Fan, X.; He, C. Enhanced Thermoelectric Performance of Conducting Polymer Composites by Constructing Sequential Energy-filtering Interfaces and Energy Barriers. *Compos. Sci. Technol.* **2022**, *221*, No. 109347.
(58) Lin, Z.; Dang, H.; Zhao, C.; Du, Y.; Chi, C.; Ma, W.; Li, Y.; Zhang, X. The Cross-interface Energy-filtering Effect at Organic/Inorganic Interfaces Balances the Trade-off Between Thermopower and Conductivity. *Nanoscale* **2022**, *14* (26), 9419−9430.

(59) Lin, Y.-C.; Huang, Y.-W.; Hung, C.-C.; Chiang, Y.-C.; Chen, C.-K.; Hsu, L.-C.; Chueh, C.-C.; Chen, W.-C. Backbone Engineering of Diketopyrrolopyrrole-Based Conjugated Polymers through Random Terpolymerization for Improved Mobility−Stretchability Property. *ACS Appl. Mater. Interfaces* **2020**, *12* (45), 50648−50659.
(60) Gayner, C.; Amouyal, Y. Energy Filtering of Charge Carriers: Current Trends, Challenges, and Prospects for Thermoelectric Materials. *Adv. Funct. Mater.* **2020**, *30* (18), No. 1901789.
(61) He, M.; Ge, J.; Lin, Z.; Feng, X.; Wang, X.; Lu, H.; Yang, Y.; Qiu, F. Thermopower Enhancement in Conducting Polymer Nanocomposites via Carrier Energy Scattering at the Organic−Inorganic Semiconductor Interface. *Energy Environ. Sci.* **2012**, *5* (8), 8351−8358.
(62) Lei, T.; Lai, Y.-C.; Hong, G.; Wang, H.; Hayoz, P.; Weitz, R. T.; Chen, C.; Dai, H.; Bao, Z. Diketopyrrolopyrrole (DPP)-Based Donor−Acceptor Polymers for Selective Dispersion of Large-Diameter Semiconducting Carbon Nanotubes. *Small* **2015**, *11* (24), 2946−2954.
(63) Zeinabad, H. A.; Zarrabian, A.; Saboury, A. A.; Alizadeh, A. M.; Falahati, M. Interaction of Single and Multi-wall Carbon Nanotubes with the Biological Systems: Tau Protein and PC12 Cells as Targets. *Sci. Rep.* **2016**, *6* (1), 26508.
(64) Spitalsky, Z.; Tasis, D.; Papagelis, K.; Galiotis, C. Carbon Nanotube-polymer Composites: Chemistry, Processing, Mechanical and Electrical Properties. *Prog. Polym. Sci.* **2010**, *35* (3), 357−401.
(65) Wang, Z.; Liu, Z.; Ning, L.; Xiao, M.; Yi, Y.; Cai, Z.; Sadhanala, A.; Zhang, G.; Chen, W.; Sirringhaus, H.; et al. Charge Mobility Enhancement for Conjugated DPP-Selenophene Polymer by Simply Replacing One Bulky Branching Alkyl Chain with Linear One at Each DPP Unit. *Chem. Mater.* **2018**, *30* (9), 3090−3100.
(66) Wood, S.; Wade, J.; Shahid, M.; Collado-Fregoso, E.; Bradley, D. D. C.; Durrant, J. R.; Heeney, M.; Kim, J.-S. Natures of Optical Absorption Transitions and Excitation Energy Dependent Photostability of Diketopyrrolopyrrole (DPP)-based Photovoltaic Copolymers. *Energy Environ. Sci.* **2015**, *8* (11), 3222−3232.
(67) Chang, L.-T.; Yu, T.-H.; Huang, H.-H.; Su, Y.-Y.; Tseng, C.-C.; Tsai, H.-J.; Hsu, W.-K. Electrolyte Adsorption Improved Thermoelectric Power of Non-conductive Polymer/Carbon Nanotubes Composites. *J. Power Sources* **2020**, *450*, No. 227651.
(68) Goldsmid, H. J. The Thermoelectric and Related Effects. In *Introduction to Thermoelectricity*, Goldsmid, H. J., Ed.; Springer: Berlin Heidelberg, 2016; pp 1−7.
(69) Zong, P.-A.; Liang, J.; Zhang, P.; Wan, C.; Wang, Y.; Koumoto, K. Graphene-Based Thermoelectrics. *ACS Appl. Energy Mater.* **2020**, *3* (3), 2224−2239.
(70) He, M.; Ge, J.; Lin, Z. Q.; Feng, X. H.; Wang, X. W.; Lu, H. B.; Yang, Y. L.; Qiu, F. Thermopower Enhancement in Conducting Polymer Nanocomposites via Carrier Energy Scattering at the Organic-Inorganic Semiconductor Interface. *Energy Environ. Sci.* **2012**, *5* (8), 8351−8358.

https://doi.org/10.1021/acsami.3c11792
ACS Appl. Mater. Interfaces 2023, 15, 56116−56126